JOURNAL OF GEOPHYSICAL RESEARCH, VOL. 87, NO. A4, PAGES 2377–2383, APRIL 1, 1982

Growth Rate Calculations of Auroral Kilometric Radiation Using the Relativistic Resonance Condition

N. OMIDI AND D. A. GURNETT

Department of Physics and Astronomy, The University of Iowa, Iowa City, Iowa 52242

The relativistic cyclotron resonance condition for right-handed extraordinary mode waves defines an ellipse in velocity space. The position of the center and size of the semiminor axis of this ellipse are functions of the plasma frequency, gyrofrequency, wave frequency, and wave normal angle. The effect of varying these parameters on the position and size of the resonance contour is analyzed. The results show that as the wave normal angle decreases, the semiminor axis increases in size and as the plasma frequency to gyrofrequency ratio decreases, the minimum energy for resonating electrons decreases and the maximum wave normal angle allowed by the resonance condition increases. Also, as the wave frequency to gyrofrequency ratio increases, the center of the resonance ellipse moves away from the origin. The relativistic resonance condition and the electron distribution in velocity space obtained by the S3-3 satellite are used to calculate numerically growth rates for the terrestrial auroral kilometric radiation. It is shown that the loss cone region of the electron distribution can give rise to growth rates for the extraordinary mode that are sufficiently large to account for the observed radio emission intensities.

1. INTRODUCTION

Spacecraft observations have revealed that auroral kilometric radiation (AKR) is the most intense of the earth's wave emissions [*Gurnett*, 1974]. The most intense component of the kilometric radiation is believed to be in the right-handed extraordinary mode [*Gurnett and Green*, 1978; *Kaiser et al.*, 1978; *Calvert*, 1981*a*]. *Melrose* [1976] proposed that kilometric radiation is generated by Doppler-shifted cyclotron resonance. Later, *Wu and Lee* [1979] suggested that relativistic effects should be included in the Doppler-shifted cyclotron resonance and that a loss cone region in the electron distribution would be unstable and give rise to AKR. In Wu and Lee's theory, the growth rate involves integration along a resonance ellipse which lies in the loss cone region. In order to locate the resonance ellipse in the loss cone region of the electron distribution, it is essential to study the roles that the wave normal angle, plasma frequency, and gyrofrequency play in determining the position and size of the resonance ellipse.

In this paper we present a detailed investigation of the relativistic cyclotron resonance condition for the free-space extraordinary mode and calculate the growth rate by using representative electron distribution functions measured in the AKR source region by the S3-3 spacecraft. We show that low-resonance energies can be obtained either near the extraordinary mode cutoff, where the index of refraction approaches zero, or at large wave normal angles. In both cases it is essential that the relativistic resonance condition be used, even for low resonance energies. By use of the S3-3 electron distribution function, two peaks occur in the growth rate. Starting from the cosmic noise background, the computed growth rates are sufficiently large to account for the observed AKR intensities, assuming representative sizes for the auroral source region.

Paper number 1A1788.
0148-0227/82/001A-1788$05.00

2. RELATIVISTIC DOPPLER-SHIFTED CYCLOTRON RESONANCE

In order for electrons with angular gyrofrequency ω_g and velocity $v_{\parallel}$ along a magnetic field line to resonate relativistically with a wave with angular frequency ω and wave normal angle θ in the observer's frame of reference, the following equation must be satisfied:

$$\omega - kv_{\parallel} \cos \theta = \frac{\omega_g}{\gamma} \tag{1}$$

where k is the wave number, $\gamma^{-1} = (1 - v^2/c^2)^{1/2}$, v is electron velocity, and c is the speed of light. Substituting $n\omega/c$ for k where n is the index of refraction and defining $Y = \omega_g/\omega$, equation (1) can be written in the following form:

$$\left[(Y^2 + n^2 \cos^2 \theta)^{1/2} v_{\parallel} - \frac{cn \cos \theta}{(Y^2 + n^2 \cos^2 \theta)^{1/2}}\right]^2 + Y^2 v_{\perp}^2 = c^2(Y^2 - 1) + \frac{c^2 n^2 \cos^2 \theta}{Y^2 + n^2 \cos^2 \theta} \tag{2}$$

where $v_{\perp}$ is electron velocity perpendicular to the magnetic field.

It is clear from the form of equation (2) that the relativistic resonance condition defines an ellipse in velocity space (Figure 1) with its center at $V_c = B/A$, semiminor axis $V_R = D/A$, and semimajor axis $V_s = D/Y$, where

$$A = (Y^2 + n^2 \cos^2 \theta)^{1/2} \tag{3a}$$

$$B = \frac{cn \cos \theta}{A} \tag{3b}$$

and

$$D^2 = c^2(Y^2 - 1) + B^2 \tag{3c}$$

Note that the relativistic resonance condition differs markedly from the nonrelativistic resonance condition, which defines a straight line in velocity space parallel to the $v_{\perp}$ axis at $v_{\parallel} = (\omega - \omega_g)/(k \cos \theta)$.

As discussed by *Stix* [1962], the index of refraction n for

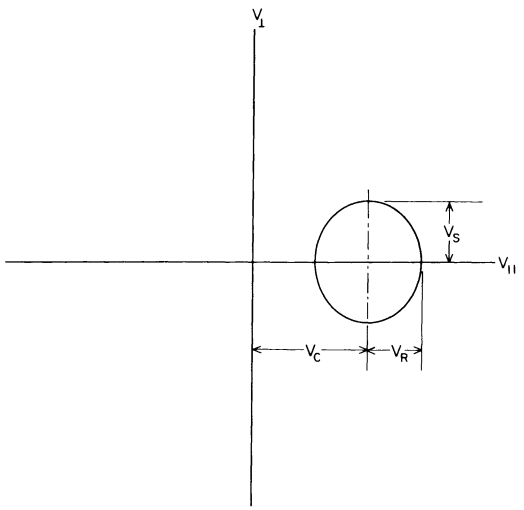

Fig. 1. Definitions of the parameters V_c, V_R, and V_s required to specify the cyclotron resonance ellipse in velocity space.

the right-handed extraordinary mode can be written in terms of X, Y, and θ, where $X = \omega_p^2/\omega^2$ and ω_p is the angular plasma frequency. Because n depends in a complicated way on the wave normal angle and the normalized plasma parameters X and Y, the resonance condition given by equation (2) is correspondingly complicated. Our first objective is to understand the dependence of the resonance condition on these parameters.

3. Size and Position of the Resonance Ellipse

Figure 2 shows V_c/c and V_R/c plotted as a function of the normalized parameter $\Delta\omega/\omega_g$ ($\Delta\omega = \omega - \omega_g$) for two ω_p/ω_g ratios and a number of wave normal angles. As can be seen, the allowed resonance conditions are bounded by the $D = 0$ boundary, which we shall now discuss. Since the semimajor and semiminor axes are given by D/Y and D/A, respectively, it is clear that when D, given by equation (3c), goes to zero the resonance ellipse shrinks to a point and disappears. Setting $D = 0$ in equation (3c) and also recalling that $V_c = B/A$, we get two equations, and by eliminating the ($n \cos \theta$) term between them we find

$$\frac{V_c}{c} = \frac{((\Delta\omega/\omega_g)(\Delta\omega/\omega_g + 2))^{1/2}}{(\Delta\omega/\omega_g) + 1} \tag{4}$$

which is the equation for the $D = 0$ boundary. Note that the $D = 0$ boundary is only a function of the ratio $\Delta\omega/\omega_g$ and is completely independent of ω_p.

The low frequency limit to cyclotron resonance occurs near the extraordinary mode cutoff, $\omega_{R=0} = \omega_g/2 + ((\omega_g/2)^2 + \omega_p^2)^{1/2}$. As this cutoff is approached from higher frequencies the index of refraction goes to zero, as illustrated in Figure 3. Near the cutoff the resonance ellipse degenerates to a circle, this time with both the radius and center shrinking to zero as ω approaches $\omega_{R=0}$. Note, however, that V_c never reaches zero because the $D = 0$ boundary is encountered before ω reaches $\omega_{R=0}$.

The bottom two panels of Figure 2 demonstrate the behavior of the semiminor axis V_R, which is equivalent to the radius of the resonance circle for low velocities. Note that for any given θ, V_R goes to zero for values of $\Delta\omega/\omega_g$ for which the V_c curve intersects the $D = 0$ boundary. Each V_c curve intersects the $D = 0$ boundary twice. Thus there are two values of $\Delta\omega/\omega_g$, marking the upper and lower bounds of the cyclotron resonance interaction region, for which $V_R = 0$.

Figures 2a and 2c indicate that as $\omega \rightarrow \omega_{R=0}$, $V_c/c \rightarrow 0$ and $V_R/c \rightarrow 0$ or in other words as $\omega \rightarrow \omega_{R=0}$ the velocity of the resonating electrons becomes very small. Thus one might think that for ω close to $\omega_{R=0}$ a nonrelativistic resonance condition might suffice. This conjecture, however, is not true for the following reason. As shown in Figure 3, the index of refraction goes to zero at $\omega_{R=0}$. By using the nonrelativistic resonance condition

$$\omega - \frac{n\omega}{c} v_{\parallel} \cos\theta = \omega_g \tag{5}$$

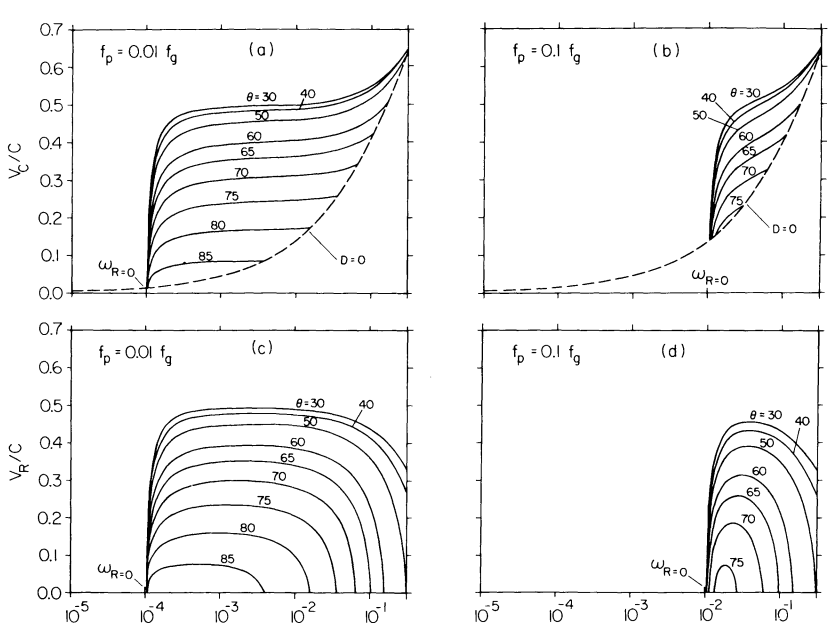

Fig. 2. V_c/c, V_R/c as functions of $(\omega - \omega_g)/\omega_g$ for two f_p/f_g ratios and a number of wave normal angles.

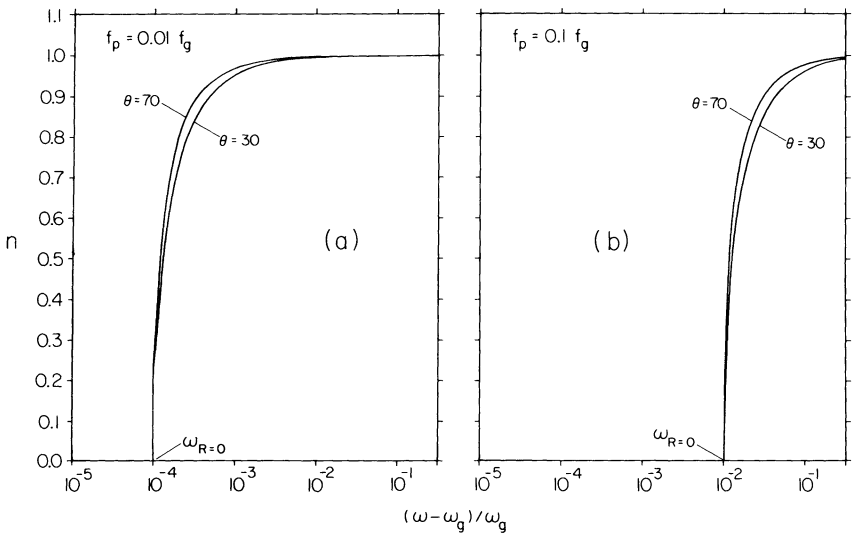

Fig. 3. Index of refraction as a function of $(\omega - \omega_g)/\omega_g$ for two f_p/f_g ratios. The index of refraction goes to zero at the extraordinary mode cutoff $\omega_{R=0}$ for all wave normal angles.

it is evident that the resonance velocity goes to infinity as $n \rightarrow 0$ or $\omega \rightarrow \omega_{R=0}$, which is in contradiction with the relativistic results. This contradiction can be resolved in the following manner. From equation (1) with $v_\perp = 0$ and the approximation $\gamma^{-1} \simeq (1 - v^2/2c^2)$, the low-velocity root for $v_\parallel$ can be written in the relativistic form as

$$\frac{v_\parallel}{c} = \frac{\omega}{\omega_g} n \cos\theta - \frac{\omega}{\omega_g} n \cos\theta \cdot \left[1 - \frac{2(\omega - \omega_g)}{\omega_g}\left(\frac{\omega_g}{\omega}\right)^2 \frac{1}{n^2 \cos^2\theta}\right]^{1/2} \quad (6)$$

If the second term in the square root is assumed to be small, then this equation reduces to the nonrelativistic resonance condition

$$\frac{v_\parallel}{c} = \frac{\Delta\omega}{\omega n \cos\theta} \quad (7)$$

whenever

$$\frac{(\omega - \omega_g)}{\omega_g}\left(\frac{\omega_g}{\omega}\right)^2 \frac{1}{n^2 \cos^2\theta} \ll 1 \quad (8)$$

It is evident, therefore, that the nonrelativistic formula for $v_\parallel$ can be obtained from the relativistic formula for $v_\parallel$ (equation (6)) if and only if equation (8) is satisfied. It is clear from equation (8) that whenever either $n \rightarrow 0$ or $\cos\theta \rightarrow 0$, the nonrelativistic formula fails to provide an adequate approximation, even for very low velocities. Recalling that $v_c/c \ll 1$ only when $n \cos\theta \ll 1$, we conclude that under no limit will the relativistic resonance ellipse approach a straight line parallel to $v_\perp$ axis, which is the nonrelativistic resonance condition.

Another dependence that can be seen from Figure 2 is that as the ω_p/ω_g ratio increases the maximum wave normal angle for which the resonance condition can be satisfied decreases and the minimum V_c increases. Thus as the ω_p/ω_g ratio decreases, the minimum energy of the resonating electrons becomes smaller.

We now illustrate the effect of $n \rightarrow 0$ and $\cos\theta \rightarrow 0$ on the resonance ellipse. One can see from equation (3*a*) that $A \rightarrow Y$ as $n \cos\theta \rightarrow 0$ or $D/A \rightarrow D/Y$, which means that as either n or $\cos\theta$ approach zero the resonance ellipse approaches a circle. Figure 4 summarizes all of the results obtained so far. For example, in Figures 4*a* and 4*c*, ω is near $\omega_{R=0}$ and thus $n \ll 1$, which explains why all the resonant curves are close to a circle. In Figures 4*b* and 4*d*, however, $n \simeq 1$, and thus the resonant curves are circular only for large wave normal angles ($\cos\theta \rightarrow 0$), and as θ becomes smaller the resonant curves become more elliptical.

Figure 5 shows the lower left part of the CMA diagram in which right-handed extraordinary mode waves exist. This illustration demonstrates how the wave normal angle determines the values of X and Y for which resonance is possible. The dashed boundary is the line on which $D = 0$ ($D = 0$ boundary), and its equation in (X, Y) space is obtained from $Y^2 + n^2 \cos^2\theta = 1$ (see equation (3*c*)) and substituting for n in terms of X, Y, and θ. Figure 5 shows that as the wave normal angle increases, a lower plasma frequency is required for resonance to occur, and that the wave frequency must be closer to cutoff frequency $\omega_{R=0}$.

Contours for the minimum energy of the resonating electrons are plotted in the CMA diagram of Figure 6. The line to which various contours are tangent is the $D = 0$ boundary. We can see that as the contours approach $D = 0$, they turn around and eventually join the $D = 0$ boundary. This is due to the sharp cutoff at $D = 0$. Therefore, the energies in the region near the $D = 0$ boundary are not represented by the contours; in other words, for any given contour, the segment between the maximum and the $D = 0$ boundary should not be considered as the correct continuation of that contour. Figure 6 shows that as the wave normal angle increases, only lower energy electrons can resonate with waves. In other words, in a region with low ω_p and ω near $\omega_{R=0}$, waves only resonate with low-energy electrons, and as the wave normal angle increases, lower plasma frequencies are required for resonance.

4. Growth Rate Calculations

Wu and Lee [1979] have suggested that a loss cone feature in the distribution of the ascending electrons in the auroral zone would give rise to instability and growth of auroral

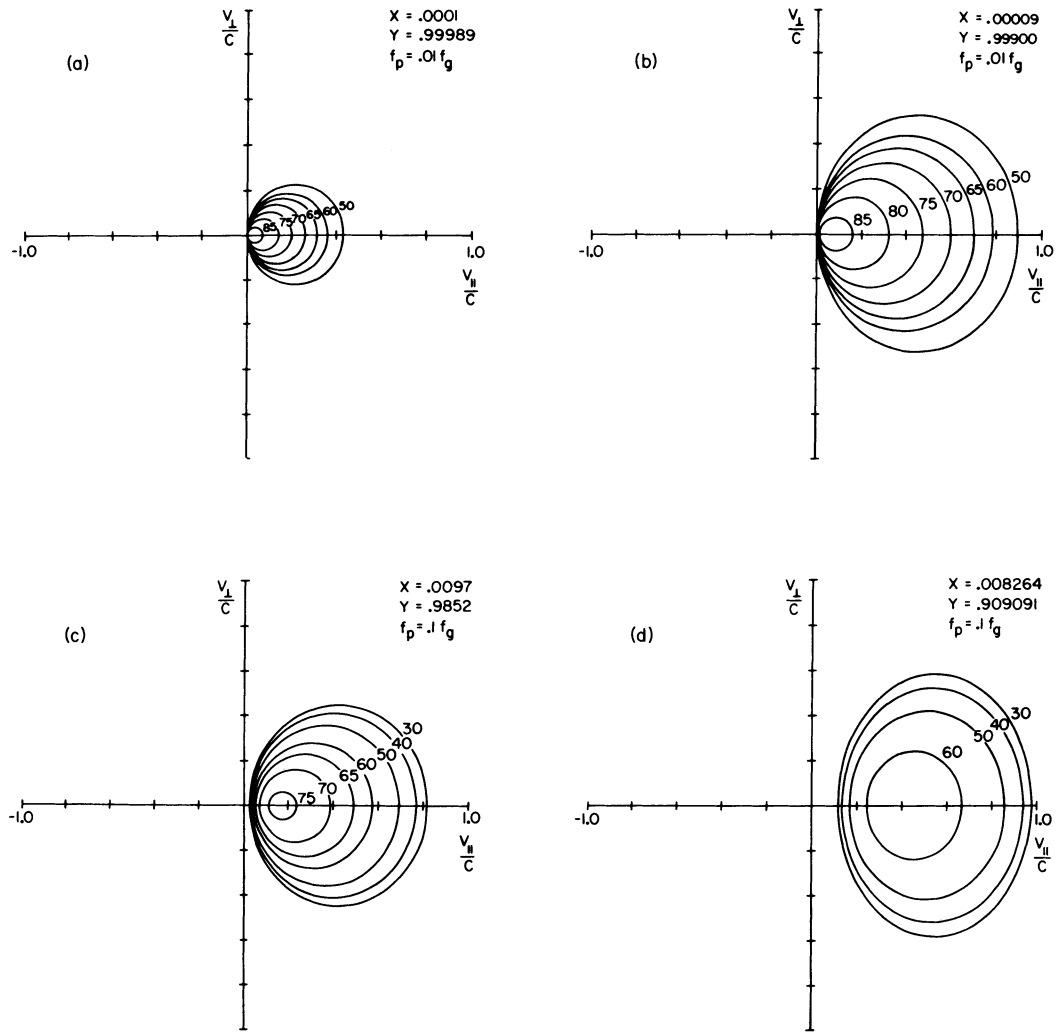

Fig. 4. Relativistic resonance ellipses in velocity space for a number of wave normal angles and two f_p/f_g ratios: ω is near $\omega_{R=0}$ in 4*a* and 4*c* but is not so close in 4*b* and 4*d*.

kilometric radiation. In their article [*Wu and Lee*, 1979], the expression for ω_i (imaginary part of the angular frequency) of the right-handed extraordinary mode is given by

$$\omega_i = \frac{\pi^2 \omega_p^2}{4\omega n_e} \int_0^\infty dv_\parallel \int_0^\infty dv_\perp v_\perp^2 \delta\left(\omega - \frac{\omega_g}{\gamma} - k_\parallel v_\parallel\right) \cdot \left(\omega_g \frac{\partial F}{\partial v_\perp} + k_\parallel v_\perp \frac{\partial F}{\partial v_\parallel}\right) \quad (9)$$

which is based on the assumption that $\omega_i \ll \omega$ and only includes the first-order cyclotron resonance term. In equation (9), n_e is the electron plasma density and F is the distribution function for the electrons. Note that F is not normalized to unity. As Wu and Lee have indicated, in the loss cone region of the electron distribution, $\partial F/\partial v_\perp$ is large and positive and therefore it can give rise to large and positive ω_i (see equation (9)). The electron distribution used in our growth rate calculations was measured by the S3-3 satellite (see Figure 8) on day 237 of 1976. This distribution was chosen for our study for two reasons. First, the observations were obtained at high altitudes (7986 km) along the

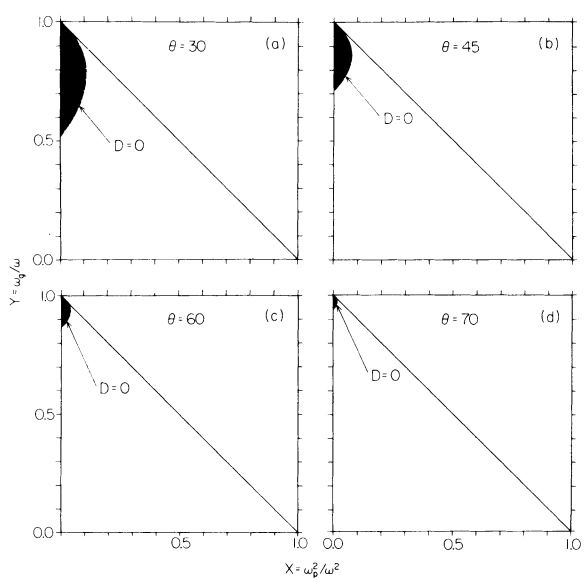

Fig. 5. Shaded areas determine values of X and Y for which resonance is possible. The shaded region is bounded by the equation $D = 0$.

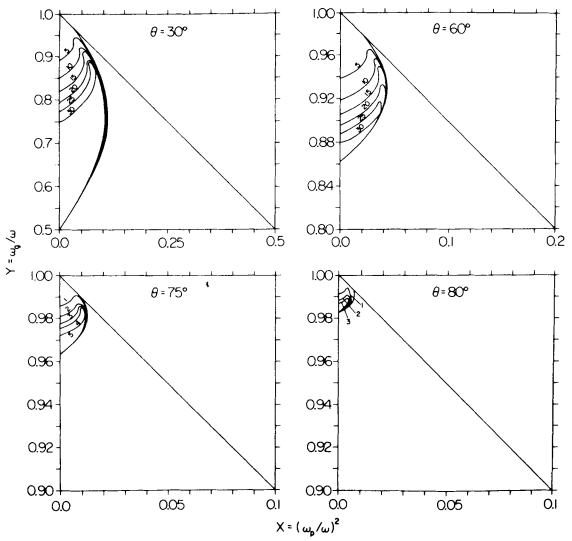

Fig. 6. Contours of minimum energy of resonating electrons in keV. All contours join the $D = 0$ boundary because of the sharp cutoff at the $D = 0$ boundary.

auroral field line in the region where the auroral kilometric radiation is believed to be generated [*Gurnett*, 1974], and second, auroral kilometric radiation was detected by the IMP 8 satellite at the same time that the electron distribution in Figure 8 was measured by S3-3. Note the pronounced loss cone feature in the electron distribution. This feature is a common characteristic of the S3-3 auroral particle observation and has been discussed by *Croley et al.* [1978].

It is clear from the delta function in equation (9) that the growth rate is determined by an integration along the resonance ellipse in velocity space. In order to carry out this integration, $\partial F/\partial v_{\parallel}$ and $\partial F/\partial v_{\perp}$ must be known along the resonance ellipse. By using the electron distribution of Figure 8, $\partial F/\partial v_{\parallel}$ and $\partial F/\partial v_{\perp}$ were numerically calculated and integrated along the resonance ellipse. To verify the accuracy of the integration routine, the growth rate was checked by using a test analytic distribution function, and the error in ω_i was found in all cases to be less than 20%. The integration errors are a combination of approximation, interpolation, and truncation errors that are involved in the numerical procedure. In Figure 7 ω_i/ω_g is plotted versus $\Delta\omega/\omega_g$ for $\theta = 80°$ and $\omega_p = 0.05\ \omega_g$, which corresponds to the density obtained by integrating the electron distribution of Figure 8, and is also in agreement with a report of a region of diminished plasma density at the AKR source region by *Calvert* [1981*b*]. We note that two regions of positive growth rate exist, separated by a region of damping. These regions are identified as regions (I), (III), and (II), respectively. In order to understand Figure 7, a point in each region was chosen (points A, B, and C), and its corresponding resonance ellipse was superimposed on the electron distribution (see Figure 8). Figures 7 and 8 clearly illustrate that when the resonance ellipse lies in the loss cone region, large positive growth rates are obtained, and when the resonance ellipse lies out of the loss cone region, negative growth rates are attained, thus verifying the expectation of Wu and Lee's theory. Having used points A, B, and C to see the effect of the location of the resonance ellipse on ω_i, we can now explain why two regions of growth and one region of damping exist in Figure 7. Very close to $\omega = \omega_{R=0}$ in Figure 7 the resonance ellipse is almost a point, as indicated before, and therefore $\omega_i \simeq 0$. As $\Delta\omega/\omega_g$ increases, V_R and V_c get larger (see Figure 2), or, in other words, the resonance ellipse begins to grow and its center moves away from the origin. Resonance ellipses corresponding to region (I) lie either completely or partially in the loss cone region of the distribution, and the contribution of positive $\partial F/\partial v_{\perp}$ in the growth rate integral is greater than the contribution of negative $\partial F/\partial v_{\parallel}$, and therefore ω_i is positive. Values of $\Delta\omega/\omega_g$ that fall in region (II) have corresponding resonance ellipses that lie partially or completely out of the loss cone region, and the contribution from negative $\partial F/\partial v_{\perp}$ is greater than the positive $\partial F/\partial v_{\perp}$ contribution, therefore, ω_i is negative. As $\Delta\omega/\omega_g$ increases beyond region (II), V_c continues to grow, however, V_R begins to shrink, with the effect that resonance ellipses corresponding to region (III) fall partially or completely in the loss cone region and, consequently, ω_i is positive again. As the frequency increases further, the radius of the resonance circle shrinks to zero at the $D = 0$ boundary and $\omega_i = 0$ above this frequency. Note that although typically three regions of growth and damping exist in the growth rate plots, there are special cases where this is not true. For example, in Figure 9 we see that there is only one region of growth in the whole frequency range for which resonance is possible. This is due to the fact that the resonance ellipses corresponding to this frequency range all lie in the loss cone region. In fact, if the wave normal angle and plasma parameters are such that the resonance ellipses never grow large enough to lie out of the loss cone region, then region (II), which corresponds to damping, will not exist and the growth rate plot will consist of one growth region only. It is clear from Figure 2 that in order for the resonance ellipses not to grow very large, the wave normal angle must be at or near the maximum wave normal angle allowed by the resonance condition. Thus for growths like that of Figure 9, it is

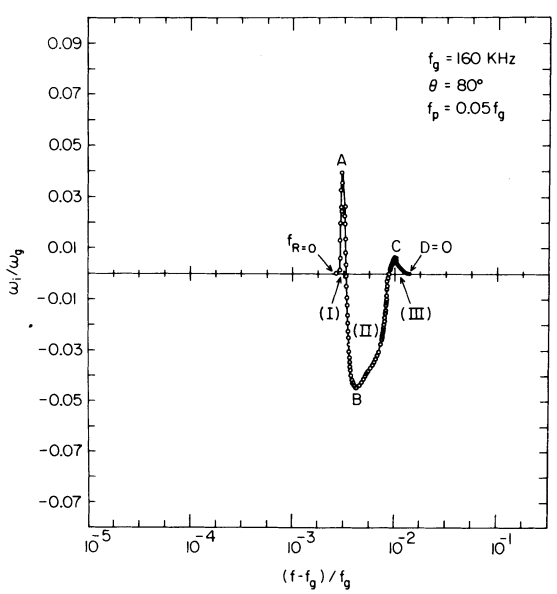

Fig. 7. Growth rates for extraordinary mode radiation computed for a representative electron distribution measured by S3-3 in the AKR source region.

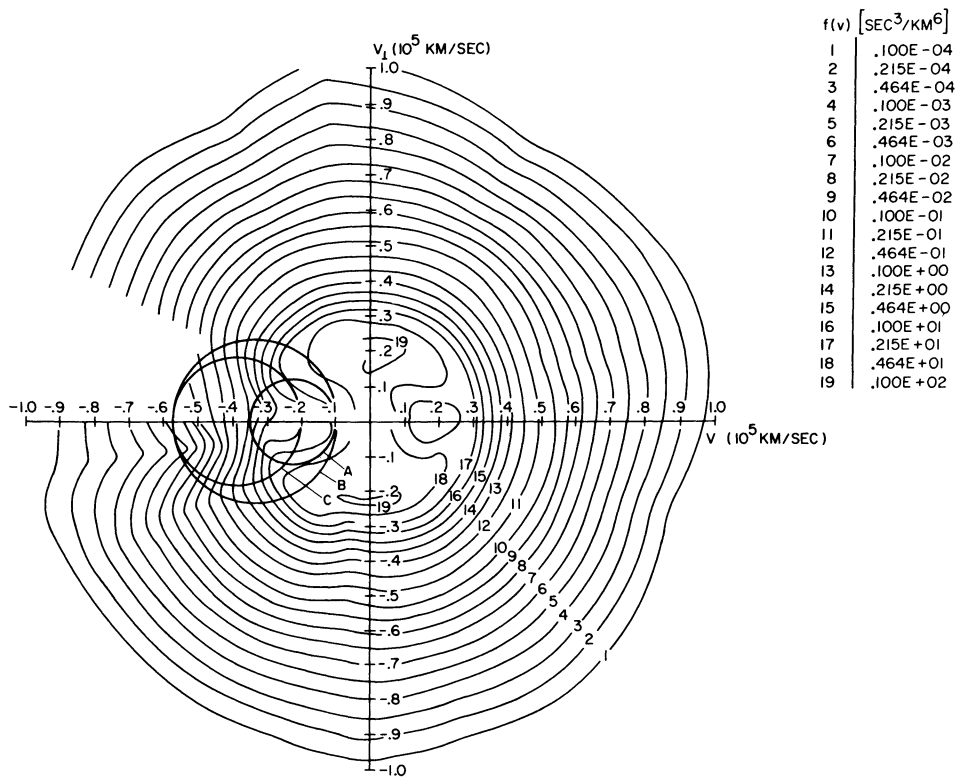

Fig. 8. The S3-3 electron distribution function used for computing the growth rates shown in Figure 7. The resonance circles labeled A, B, and C correspond to the regions (I), (II), and (III) indicated in Figure 7.

necessary but not sufficient to have large wave normal angles.

Next, we attempt to estimate the ray path length required to account for the observed AKR intensities. The most likely candidate for the input waves that are amplified into the auroral kilometric radiation is the cosmic noise background. From the cosmic noise intensity measurements of *Brown* [1973], we estimate that growth of the cosmic noise background by a factor of e^{10} should be sufficient to account for the observed AKR intensities. By using an average group velocity v_g of 8.45×10^2 km/s and average growth rate of 2.01×10^4 s^{-1} in region (I) of Figure 7, a path length of 420 m is required for growth by a factor of e^{10}. Taking $v_g = 8.5 \times 10^3$ km/s and $\omega_i = -2.26 \times 10^4$ s^{-1} for region (II), the waves will attenuate by a factor of e^{10} in 3.75 km, and finally, assuming $v_g = 3.14 \times 10^4$ km/s and $\omega_i = 3.77 \times 10^3$ s^{-1} in region (III), a path length of 83 km is required for growth by a factor of e^{10}. Since the observed size of the auroral arcs is about 100 km, one might estimate the size of the AKR source region to be about 100 km. If this is true, then it becomes clear that the obtained growth rates are large enough to account for the observed AKR intensities. It should be noted, however, that as waves grow in region (I), they must propagate through region (II) and thus undergo a strong attenuation before they grow again in region (III). Thus one advantage of special cases like that of Figure 9 is that waves do not have to go through a damping region. Of course, it goes without saying that without ray tracing one could only speculate on the growth lengths and the relative importance of each region in Figure 7. We plan to perform such ray tracings in the near future.

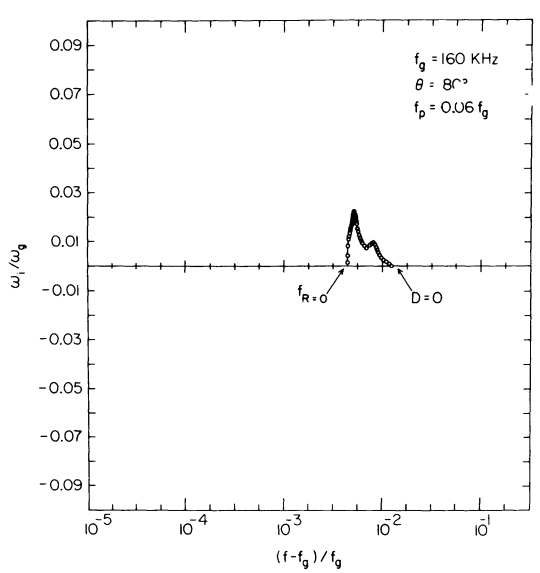

Fig. 9. Growth rates for extraordinary mode radiation corresponding to the case where the resonance ellipses never lie out of the loss cone region.

Figure 7 was plotted keeping θ and ω_g constant and varying ω. Another way of looking at Figure 7, however, would be to consider θ and ω constant and ω_g varying. The result would be very similar to Figure 7, and the only difference would stem from the fact that in equation (9), ω would stay constant rather than varying as is the case in Figure 7, but since the values of ω and ω_g are close, the change in Figure 7 would be very small. It was suggested by *Calvert* [1981*a*], using a refraction model, that in the AKR source region waves with the same frequency originating at different altitudes (thus different ω_g) would have different ray

paths and would form a hollow emission cone. Keeping this in mind, Figure 7 would predict a hollow emission cone, since growth occurs at certain intervals of ω_g. At this point, however, the authors feel more study of this matter is required before conclusively accepting or rejecting this idea.

5. Conclusions

In this paper we have discussed the relativistic Doppler-shifted cyclotron resonance, and it has been shown that this resonance condition defines an ellipse in the velocity space. The dependence of the size and position of the resonance ellipse on the wave frequency, gyrofrequency, plasma frequency, and wave normal angle has been explored. We have shown that for a given θ and ω_p/ω_g ratio there exists a certain frequency range for which resonance is possible and outside of which resonance does not occur. This frequency range is bounded by the $D = 0$ boundary, whose equation in $(v_c/c, \Delta\omega/\omega_g)$ space is independent of ω_p. The plasma frequency to gyrofrequency ratio determines the maximum wave normal angle allowed by the resonance condition, and it also determines the minimum energy of the resonating electrons. As the ω_p/ω_g ratio gets smaller, the maximum wave normal angle allowed gets larger and the minimum energy of the resonating electrons becomes smaller. We have also demonstrated that for either $n \to 0$ or $\cos\theta \to 0$ the nonrelativistic cyclotron resonance cannot be approximated by the relativistic cyclotron resonance condition. Because the relativistic cyclotron resonance predicts small velocities for the resonating electrons only when $n \times \cos\theta \to 0$, we conclude that the nonrelativistic cyclotron resonance should not be used for the right-handed extraordinary mode waves.

By using the expression for ω_i given by *Wu and Lee* [1979] and an electron distribution function measured in the AKR source region by S3-3 satellite, we have calculated growth rates for auroral kilometric radiation and have demonstrated that the loss cone region of the electron distribution is unstable, as predicted by Wu and Lee. A plot of ω_i/ω_g versus $\Delta\omega/\omega_g$ has defined three separate regions on $\Delta\omega/\omega_g$ axis, two of which are growth regions and one of which is a damping region. One growth region occurs very close to the extraordinary mode cutoff, and the second occurs at large wave normal angles. Starting from the cosmic noise background, ray path lengths of 420 m and 83 km are needed for these two growth regions, respectively, to account for the observed kilometric radiation intensities.

Acknowledgments. The authors would like to thank D. R. Croley for providing them with S3-3 electron distribution data and W. Calvert for helpful discussions and suggestions. This research was supported by National Aeronautics and Space Administration grant NGL-16-001-043.

The Editor thanks S. A. Curtis and C. S. Wu for their assistance in evaluating this paper.

References

Brown, L. W., The galactic radio spectrum between 130 kHz and 2600 kHz, *Astrophys. J., 180,* 359, 1973.

Calvert, W., The signature of auroral kilometric radiation on ISIS 1 ionograms, *J. Geophys. Res., 86,* 76–82, 1981*a*.

Calvert, W., The auroral plasma cavity, *Geophys. Res. Lett., 8,* 919, 1981*b*.

Croley, D. R., P. F. Mizera, and J. F. Fennel, Signature of a parallel electric field in ion and electron distributions in velocity space, *J. Geophys. Res., 83,* 2701–2705, 1978.

Gurnett, D. A., The earth as a radio source: Terrestrial kilometric radiation, *J. Geophys. Res., 79,* 4227–4238, 1974.

Gurnett, D. A., and J. L. Green. On the polarization and origin of auroral kilometric radiation, *J. Geophys. Res., 83,* 689–696, 1978.

Kaiser, M. L., J. K. Alexander, A. C. Riddle, J. B. Pearce, and J. W. Warwick, Direct measurements of the polarization of terrestrial kilometric radiation from Voyagers 1 and 2, *Geophys. Res. Lett., 5,* 857, 1978.

Melrose, D. B., An interpretation of Jupiter's radiation and the terrestrial kilometric radiation as direct amplified gyroemission, *Astrophys. J., 207,* 651, 1976.

Stix, T. H., *The Theory of Plasma Waves,* McGraw-Hill, New York, 1962.

Wu, C. S., and L. C. Lee, A theory of the terrestrial kilometric radiation, *Astrophys. J., 230,* 621–626, 1979.

(Received September 16, 1981;
revised November 19, 1981;
accepted November 19, 1981.)